frontiers in Earth Science

ORIGINAL RESEARCH
published: 03 December 2020
doi: 10.3389/feart.2020.585770

Holocene Hydroclimate Variability and Vegetation Response in the Ethiopian Highlands (Lake Dendi)

Andrea Jaeschke[1], Matthias Thienemann[1], Enno Schefuß[2], Jonas Urban[3], Frank Schäbitz[3], Bernd Wagner[1] and Janet Rethemeyer[1]*

[1]Institute of Geology and Mineralogy, University of Cologne, Cologne, Germany, [2]MARUM-Center for Marine Environmental Sciences, University of Bremen, Bremen, Germany, [3]Institute of Geography Education, University of Cologne, Cologne, Germany

Northern Africa's past climate is characterized by a prolonged humid period known as the African Humid Period (AHP), giving origin to the "Green Sahara" and supporting human settlements into areas that are now desert. The spatial and temporal extent of climate change associated with the AHP is, however, subject to ongoing debate. Uncertainties arise from the complex nature of African climate, which is controlled by the strength and interactions of different monsoonal systems, resulting in meridional shifts in rainfall belts and zonal movements of the Congo Air Boundary. Here, we examine a ~12,500-years record of hydroclimate variability from Lake Dendi located in the Ethiopian highlands based on a combination of plant-wax-specific hydrogen (δD) and carbon ($\delta^{13}C$) isotopes. In addition, pollen data from the same sediment core are used to investigate the response of the regional vegetation to changing climate. Our δD record indicates high precipitation during peak AHP (ca. 10 to 8 ka BP) followed by a gradual transition toward a drier late Holocene climate. Likewise, vegetation cover changed from predominant grassland toward an arid montane forest dominated by *Juniperus* and *Podocarpus* accompanied by a general reduction of understory grasses. This trend is corroborated by $\delta^{13}C$ values pointing to an increased contribution of C_3 plants during the mid-to late Holocene. Peak aridity occurred around 2 ka BP, followed by a return to a generally wetter climate possibly linked to enhanced Indian Ocean Monsoon strength. During the last millennium, increased anthropogenic activity, i.e., deforestation and agriculture is indicated by the pollen data, in agreement with intensified human impact recorded for the region. The magnitude of δD change (40‰) between peak wet conditions and late Holocene aridity is in line with other regional δD records of East Africa influenced by the CAB. The timing and pace of aridification parallels those of African and Indian monsoon records indicating a gradual response to local insolation change. Our new record combining plant-wax δD and $\delta^{13}C$ values with pollen highlights the sensitive responses of the regional vegetation to precipitation changes in the Ethiopian highlands.

Keywords: African Humid Period, Ethiopia, Lake Dendi, n-alkanes, δD, $\delta^{13}C$, pollen

OPEN ACCESS

Edited by:
David K. Wright,
University of Oslo, Norway

Reviewed by:
Nadia Solovieva,
University College London,
United Kingdom
Chengyu Weng,
Tongji University, China

****Correspondence:***
Andrea Jaeschke
andrea.jaeschke@uni-koeln.de

Specialty section:
This article was submitted to Quaternary Science, Geomorphology and Paleoenvironment, a section of the journal Frontiers in Earth Science

Received: *21 July 2020*
Accepted: *11 November 2020*
Published: *03 December 2020*

Citation:
Jaeschke A, Thienemann M, Schefuß E, Urban J, Schäbitz F, Wagner B and Rethemeyer J (2020) Holocene Hydroclimate Variability and Vegetation Response in the Ethiopian Highlands (Lake Dendi). Front. Earth Sci. 8:585770. doi: 10.3389/feart.2020.585770

1. INTRODUCTION

North Africa experienced extreme climatic variations during the Holocene with a prolonged humid period known as the African Humid Period (AHP), which had major consequences for terrestrial ecosystems and ancient civilizations (see recent review by Pausata et al., 2020). During this humid period, increased Northern Hemisphere (NH) summer insolation induced the northward extension and intensification of the tropical rainbelt (Gasse, 2000; Lézine et al., 2011a). Remains of large palaeo-lakes and -estuaries across northern Africa record the substantially altered hydroclimate during the AHP, which transformed the Saharan desert into an open grass savannah and allowed for widespread human occupation of nowadays mostly barren landscapes (Lézine et al., 1990; Kuper and Kröpelin, 2006; Kröpelin et al., 2008; Sereno et al., 2008; Tierney et al., 2017; Höpker et al., 2019). The subsequent return to arid climate is assumed to explain major societal shifts, including the demise of the Egyptian Old Kingdom, attributed to dramatic failure of annual Nile River floods driven by declining rainfall in the Ethiopian highlands (Stanley et al., 2003; Kuper and Kröpelin, 2006).

The timing and extent of the transition between the "Green Sahara" and today's hyperarid desert at the end of the AHP is, however, still highly debated. While many records suggest a gradual or time-transgressive transition (Kröpelin et al., 2008; Lézine et al., 2011b; Berke et al., 2012b; Foerster et al., 2012; Shanahan et al., 2015; Castañeda et al., 2016; Tierney et al., 2017) toward peak aridity at about 2–4 ka BP as a linear response to radiative forcing, others indicate an abrupt end of the AHP triggered by nonlinear biogeophysical feedback processes (DeMenocal et al., 2000; Claussen et al., 2013; Tierney and deMenocal, 2013; Collins et al., 2017). Uncertainties in the reconstructions arise from complex patterns of convergence and precipitation associated with both Atlantic and Indian Ocean climate dynamics as well as extratropical teleconnections shaping North African hydroclimate (Camberlin et al., 2001; Nicholson, 2017). Therefore, changes in the locations of the Intertropical Convergence Zone (ITCZ) and associated monsoonal rainfall belts as well as the Congo Air Boundary (CAB) may affect sedimentary archives differently, in particular in the easternmost sector of tropical Africa (Tierney et al., 2010; Tierney et al., 2011; Foerster et al., 2012; Costa et al., 2014; Junginger et al., 2014; Wagner et al., 2018). Further complications arise from the different sensitivity of individual hydroclimate proxies (Castañeda et al., 2016).

Because of their specificity as a plant biomarker, long-chain *n*-alkanes are well suited for reconstructing climate and ecosystem changes recorded in lacustrine sediments (e.g., Eglinton and Eglinton, 2008; Castañeda and Schouten, 2011). Sedimentary leaf-wax *n*-alkane δD values (δD_{wax}) have been frequently used to reconstruct past changes in the hydrological cycle (Schefuß et al., 2005; Tierney et al., 2010; Berke et al., 2012b; Kuechler et al., 2013; Costa et al., 2014; Castañeda et al., 2016; Collins et al., 2017). In tropical regions with only minor temperature variations, the most prominent factor influencing δD_{wax} is the amount effect (Bowen, 2008; Sachse et al., 2012). Apart from precipitation amounts, shifting wind regimes and associated variations in moisture sources have a strong control on δD_{wax} in East Africa (Levin et al., 2009; Costa et al., 2014; Castañeda et al., 2016). In addition, changes in vegetation type, carbon fixation pathways and relative humidity can exert secondary effects on δD_{wax} (Smith and Freeman, 2006; Sachse et al., 2012; Kahmen et al., 2013). Sedimentary $\delta^{13}C$ values ($\delta^{13}C_{wax}$) have also been shown to be sensitive to environmental conditions (i.e., temperature, rainfall) and are used as proxies for continental vegetation (C_3 vs. C_4 plant types) and climate change (Schefuß et al., 2003; Schefuß et al., 2005; Castañeda et al., 2009; Berke et al., 2012b; Kuechler et al., 2013; Dupont and Schefuß, 2018).

Previous studies from East African lakes using the same molecular approach (δD_{wax}, $\delta^{13}C_{wax}$) also exhibited significant differences in hydroclimate changes particularly in the timing of the AHP termination, i.e. abrupt vs. gradual (Tierney et al., 2010; Tierney et al., 2011; Berke et al., 2012b; Costa et al., 2014). This non-uniform hydroclimate response on a regional scale may relate to locally different precipitation regimes (bimodal vs. unimodal), humidity sources (Atlantic Ocean vs. Indian Ocean) modulated by the zonal movement of the CAB (Tierney et al., 2011; Costa et al., 2014; Junginger et al., 2014), and topography. Moreover, local vegetation structure may respond differently to regionally changing moisture balance (Lézine et al., 2011b; Berke et al., 2012b; Sachse et al., 2012; Kuechler et al., 2013). Information about vegetation composition is, however, missing in most of the previous investigations. In this study, we provide new insights into the termination of the AHP based on a sediment core from Lake Dendi located in the central Ethiopian highlands (2,836 m asl), where recent archaeological investigations indicated a long history of human occupation (Vogelsang et al., 2018). We use δD_{wax} to assess the regional precipitation history, and $\delta^{13}C_{wax}$ to examine the distribution of C_3 and C_4 vegetation in the catchment. In addition, we assess variations in pollen abundances to investigate the response of regional vegetation structure to changes in hydroclimate. A preceding study by Wagner et al. (2018) focused on sedimentological data to reconstruct erosion and rainfall dynamics in the lake catchment. According to this study, most arid conditions were reached at 3.9 ka BP but relatively stable climate conditions with low erosion and few rainfall events were indicated throughout the mid Holocene. The combination of molecular records with pollen data applied in this study allows a more differentiated perspective of environmental change at this high-altitude location over the past 12,500 years.

2. MATERIALS AND METHODS

2.1. Study Area and Climate Background

Lake Dendi is located on the central Ethiopian Plateau (8°50'N, 38°02'E; 2,836 m elevation) about 80 km to the west of Addis Ababa (**Figure 1A**). The lake is situated inside an ~8-km wide caldera of the dormant volcano Mount Dendi (**Figure 1B**). It comprises two basins connected via a shallow sill and has a maximum water depth of ~56 m in the eastern basin (Wagner

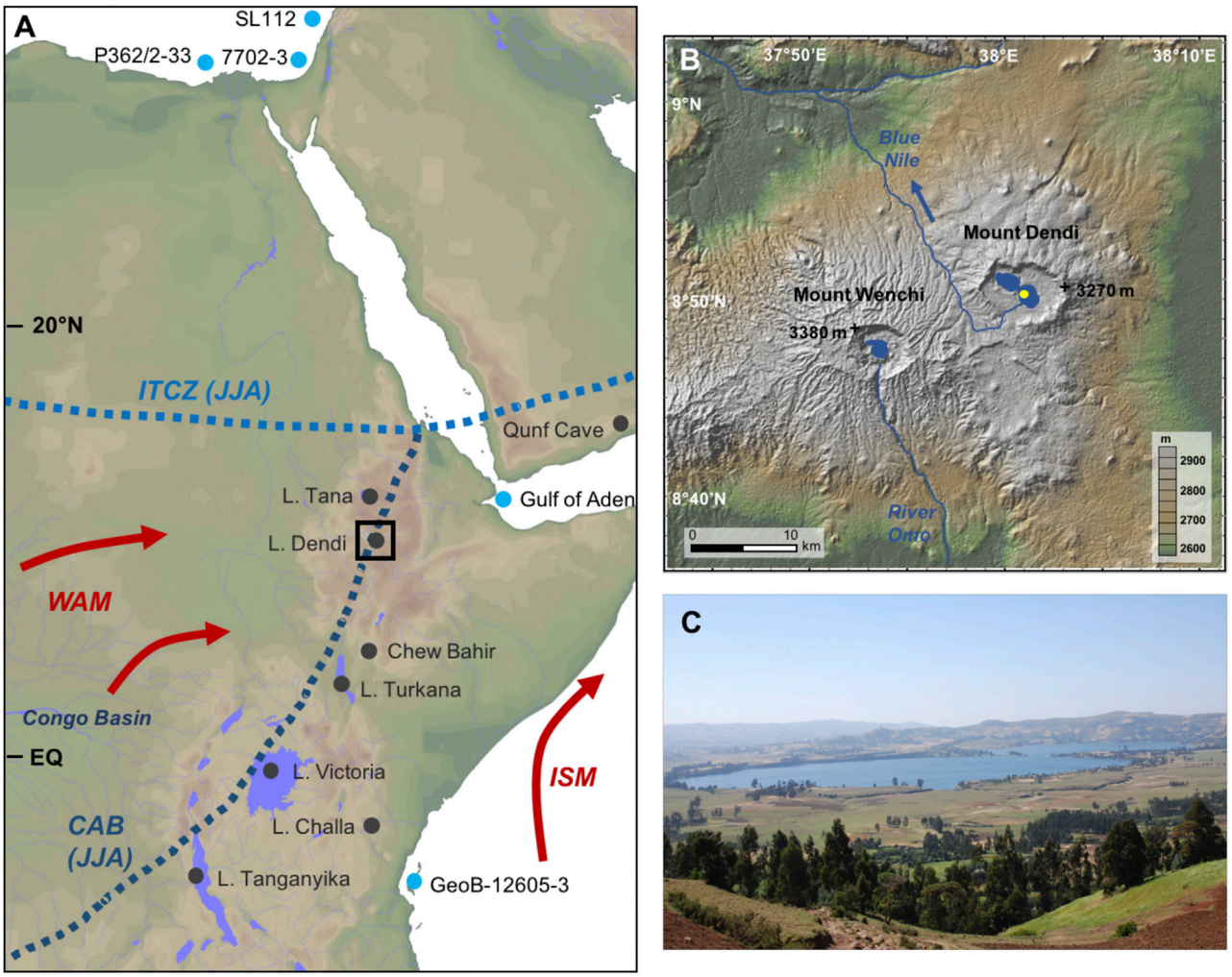

FIGURE 1 | (A) Map of Northeast Africa with the positions of terrestrial (black dots) and marine archives (blue dots) mentioned in the text. The black box denotes the Lake Dendi region. The approximate locations of the Intertropical convergence zone (ITCZ) and Congo Air Boundary (CAB) during northern hemisphere summer are indicated by blue dotted lines. Red arrows illustrate pathways of moisture advected from the Atlantic Ocean/Congo Basin and Indian Ocean during summer monsoon (WAM: West African Monsoon; ISM: Indian Summer Monsoon) **(B)** Close-up of the study area on the central Ethiopian Plateau showing the Dendi crater and coring location in the eastern lake (yellow dot). Lake Dendi seasonally contributes to the drainage system of the Blue Nile (indicated by blue arrow). Mount Wenchi is located about 12 km to the southwest. **(C)** The photograph shows the view from the northeastern crater rim on the two basins of Lake Dendi and the local vegetation, which is at present influenced by anthropogenic activity.

et al., 2018). The temperature of the upper 40 m of the oligotrophic lake ranges between 15° and 16°C (Degefu et al., 2014). Lake Dendi lacks permanent surface inlets but is fed by numerous small rivers and streams during the rainy season. The seasonally active outlet in the southwestern corner of the lake (**Figure 1B**) contributes to the drainage system of the Blue Nile (Degefu et al., 2014; Wagner et al., 2018). The lake catchment is part of the Lower Dega region, which is characterized by a sub-humid climate with moderate seasonal temperatures ranging from 14°C in winter to 17°C in summer (Mitchell and Jones, 2005).

The hydroclimate in the study area is controlled by the African rainbelt, which is closely associated with the ITCZ (**Figure 1A**). Both migrate seasonally between ca. 20°N (July) and ca. 20°S (January), following the movement of the insolation maximum (Nicholson, 2000). Another zone of convergence, the CAB, separates air masses containing moisture derived from the Atlantic and Indian Ocean (Mitchell and Jones, 2005; Degefu et al., 2014; Nicholson, 2017). Generation of rainfall and the seasonal shift of the African rainbelt are also closely linked to seasonally varying monsoon winds, which bring humid (dry) air on land during the summer (winter) months (Nicholson, 2000; Trenberth et al., 2000). A main rainy season from June to September is caused by movement of the rainbelt to its northernmost position. Highest rainfall (>250 mm/month) is observed during July and August, when the CAB allows moisture from westerly sources (i.e., Congo Basin) to reach the area (Mitchell and Jones, 2005; Levin et al., 2009). This

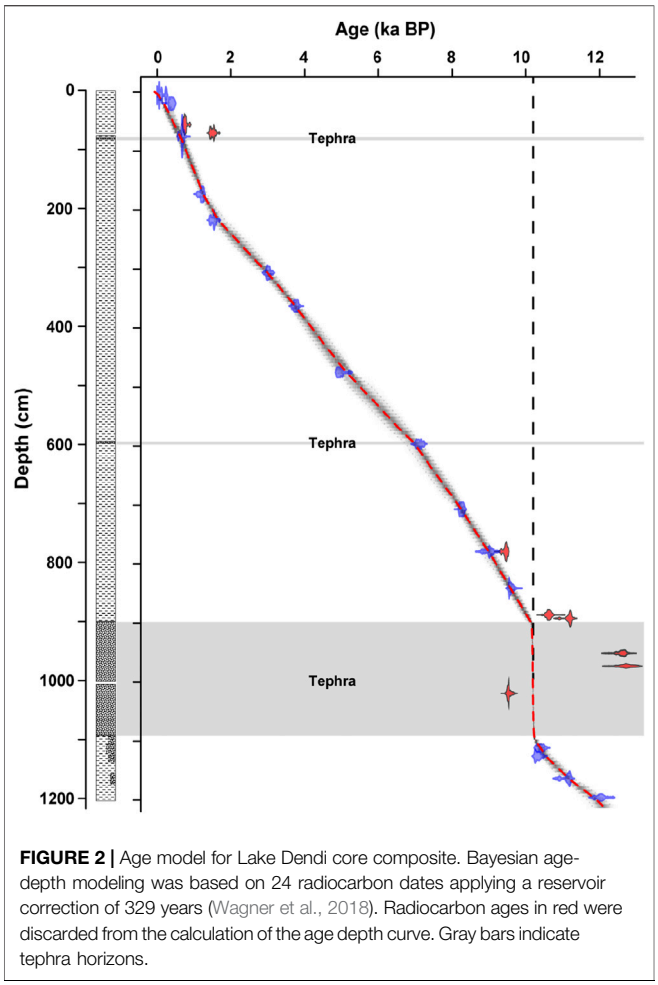

FIGURE 2 | Age model for Lake Dendi core composite. Bayesian age-depth modeling was based on 24 radiocarbon dates applying a reservoir correction of 329 years (Wagner et al., 2018). Radiocarbon ages in red were discarded from the calculation of the age depth curve. Gray bars indicate tephra horizons.

Congo Basin sourced precipitation is assumed to be more D-depleted compared to that from the Indian Ocean and may thus impact the isotopic composition of rainfall in Ethiopia (Levin et al., 2009; Costa et al., 2014). A relatively dry season (<50 mm/month) between October and February is characterized by predominant northeasterly winds. Rainfall during the short rain season in October-November is related to sea surface temperature (SST) anomalies, with intensified rains during periods of anomalous high SST in the western Indian Ocean (Nicholson, 2000; Ummenhofer et al., 2009). During February/March to May, prevailing easterly and southeasterly winds from the Indian Ocean cause the spring rainy season in the central Ethiopian highlands (Levin et al., 2009). Annual precipitation in the Dendi region averages ~1,200 mm (Mitchell and Jones, 2005; Degefu et al., 2014).

The natural vegetation in the catchment of Lake Dendi can be assigned to the "dry evergreen Afromontane forest" (Bekele, 1993; Friis et al., 2011), representing a mixture of open forest with dominant conifers, Juniper trees, and African redwood, interspersed with high-mountain grassland, mosses and lichens (Friis 1992; Bonnefille and Mohammed, 1994; Darbyshire et al., 2003). Today's landscape, however, is characterized by anthropogenic influence through deforestation and intensive agricultural activity that largely replaced the natural vegetation (**Figure 1C**) (Darbyshire et al., 2003; Hailu et al., 2015; Wagner et al., 2018). Archaeological investigations indicated human activity in the area of the Dendi caldera already more than 200 ka ago, and the crater lakes may have been important water reservoirs during more arid periods in the past, while the obsidian resource might have been important for the preparation of stone tools (Vogelsang et al., 2018).

Two sediment cores (DEN1: 08°50.178'N, 38°00.974'E and DEN2: 08°50.153'N, 38°01.075'E; **Supplementary Figure S1**) were obtained from the eastern twin-lake from a water depth of 50 and 54 m, respectively, in spring 2012. The cores were correlated based on optical and XRF analyses. Bayesian age-depth modeling used 24 radiocarbon (^{14}C) ages and provided a basal age of 12.19 cal ka BP for the correlated core (Wagner et al., 2018) (**Figure 2**). A reservoir correction of 329 years was applied to the entire set, consisting exclusively of bulk organic carbon samples. Sampling for molecular analyses was done with a resolution of ~200 years, and excluding the tephra. Detailed information on the age model can be found in Wagner et al. (2018).

2.2. Lipid Biomarker Extraction and Fractionation

Freeze dried sediment samples (ca. 2–7 g) were ultrasonically extracted with dichloromethane (DCM)/methanol (9:1, v/v) for 5 min repeated 3 times. The extracts were combined and the bulk of the solvent subsequently removed by rotary evaporation under vacuum. The resulting total lipid extracts (TLE) were saponified using 0.5 M aqueous potassium hydroxide (KOH) solution at 80°C for 2 h. Non-saponifiable lipids (neutral lipids) were extracted out of the basic solution using *n*-hexane. The neutral fractions were chromatographically separated using activated silica gel and *n*-hexane and DCM/methanol (1:1, v/v) to elute apolar and polar compounds, respectively. The apolar fractions were further separated into saturated and unsaturated compounds using $AgNO_3$-coated silica gel and *n*-hexane and DCM, respectively.

2.3. Sediment *n*-Alkane Analysis

n-Alkanes were analyzed using a gas chromatograph equipped with an on-column injector and a flame ionization detector (GC-FID; HP 5890). A fused silica capillary column (DB-5MS; 50 m × 0.2 mm, film thickness: 0.33 μm) was used with He as carrier gas. Samples were injected at 70°C and the GC oven temperature was subsequently raised to 150°C at a rate of 20°C/min, and then at 6°C/min to 320°C (held 40 min). Identification of *n*-alkanes was based on retention time in comparison with those of a standard solution (*n*-C_{21}–*n*-C_{40}). Analytical precision of the *n*-alkane quantifications based on replicate standard analyses was <5%.

To distinguish between contributions of higher plant wax and petrogenic sources, the carbon preference index (CPI; Bray and Evans, 1961) was calculated using the abundances of odd- and even-numbered *n*-alkane chain lengths from C_{27} to C_{33}:

$$CPI_{27-33} = 0.5 \times \left(\frac{nC_{27} + nC_{29} + nC_{31} + nC_{33}}{nC_{26} + nC_{28} + nC_{30} + nC_{32}} + \frac{nC_{27} + nC_{29} + nC_{31} + nC_{33}}{nC_{28} + nC_{30} + nC_{32} + nC_{34}} \right)$$

2.4. Compound-specific δD and $\delta^{13}C$ Analysis

δD analysis of the most abundant *n*-alkane homologues (*n*-C_{29} and *n*-C_{31}) was performed on a Thermo Trace GC coupled via a pyrolysis reactor to a Thermofisher MAT 253 mass spectrometer (GC/IR-MS) according to Jaeschke et al. (2018). The GC was equipped with a 30 m × 0.25 mm column (Restek Rxi-5ms, film thickness: 1.0 µm) and He was used as the carrier gas. The samples were injected via a PTV injector at 40°C and then transferred to the GC column. The GC temperature was programmed to increase from 120°C (2 min hold) to 200°C at 30°C/min and then at 4°C/min to 320°C (held 12.3 min). δD values were measured against calibrated reference gas using H_2 and are reported in ‰ relative to Vienna Standard Mean Ocean Water (VSMOW). The H_3-factor had a mean of 6.00 ± 0.02. An external standard mixture with known δD values was analyzed repeatedly in between samples and yielded a long-term precision of <3‰ and a mean deviation of <1‰ from reference values. All samples were analyzed in duplicate with an average standard deviation of 2‰.

$\delta^{13}C$ analysis of long chain *n*-alkanes was performed using a Trace GC instrument equipped with a 30 m × 0.25 mm column (Restek Rxi-5ms, film thickness: 0.25 µm) coupled via a combustion interface to a Thermofisher MAT 252 MS. He was used as carrier gas. The samples were injected via a PTV injector at 40°C and then transferred to the GC column. The GC oven was programmed from 60°C (3 min hold) to 150°C at 20°C/min, and then at 4°C/min to 320°C (held 10 min). Quantitative conversion of eluting compounds to CO_2 was conducted in a ceramic tube filled with Ni wires at 1,000°C using a trickle flow of O_2. CO_2 gas of known isotope composition was used as reference gas and $\delta^{13}C$ values are reported in ‰ relative to Vienna Peedee Belemnite (VPDB). Repeated analysis of an external *n*-alkane standard yielded long-term accuracy and precision of <0.1 and 0.3‰, respectively. All samples were analyzed in duplicate with an average standard deviation of 0.2‰.

2.5. Pollen Analysis

21 horizons, deriving from 64 cm equidistance core samples, were selected for pollen analysis. From each horizon, 2 cm^3 sediment material was used for laboratory preparation according to standard procedures including acetolysis (Faegri et al., 1989). Firstly, 10% HCl was added to remove $CaCO_3$. After washing with water and before sieving the remaining sample through a 112 µm wide mesh, 10% KOH was used to diminish organic material. Then 40% HF destroyed the sand grains before acetolysis (9 ml acetic anhydride and 1 ml concentrated sulfuric acid) decomposed cellulose. Finally, clay particles were washed out carefully in an ultrasonic bath. One drop of the remaining material was mounted on a microscope slide. The counting of the pollen grains was done under a Zeiss Primo Star light microscope using 400 to 1,000 times magnification until 300 individual grains were determined. To identify the taxonomic affiliation of each grain, photos, description and pollen atlases were used (Bonnefille 1971a; Bonnefille 1971b; Bonnefille and Riollet, 1980; Hamilton, 1982). The non-palynomorphes were identified with the help of Gelorini et al. (2011) and Van Geel et al. (2011). The concentration of spores was calculated using known numbers of *Lycopodium* markers in a tablet added to the samples before processing. The pollen diagram was constructed using the TILIA software, version 2.0.41 (Grimm, 2015). Cyperaceae were excluded from the pollen sum as they are generally limited to lake margins and thus not representative for the broader regional vegetation. For the zonation of the diagram, CONISS ("Constrained cluster analysis by sum-of-squares") analysis, was used including terrestrial pollen grains appearing at least once with more than 5%.

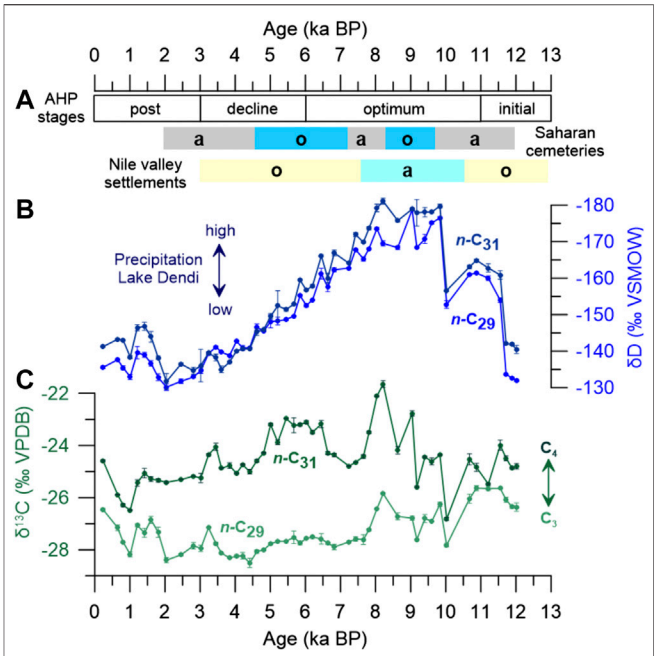

FIGURE 3 | Timing of the stages of the African Humid Period (AHP) based on paleohydrological records in northern Africa (10–25°N; Lézine et al., 2011a). Archaeological evidence for prehistoric human occupation of the Sahara (paleolake Gobero, Niger; Sereno et al., 2008) and the Nile valley (Kuper and Kröpelin, 2006; Weldeab et al., 2014). **(A)** Colored bars indicate phases of occupation (o) and abandonment (a), blue colours indicate humid phases. **(B)** δD values of the n-C_{29} (light blue) and n-C_{31} (dark blue) homologues from Lake Dendi sediment core. **(C)** $\delta^{13}C$ values of the n-C_{29} (light green) and n-C_{31} (dark green) homologues from Lake Dendi sediment core. Error bars represent analytical precision.

3. RESULTS

3.1. *n*-Alkane Distributions

The *n*-alkane distribution in all sediment samples shows a strong odd over even predominance with highest abundances of the *n*-C_{29} and *n*-C_{31} homologues. The C_{29} *n*-alkane is in general more

dominantly produced by trees and shrubs (C_3 photosynthesis), while the C_{31} *n*-alkane is more evenly produced by trees (C_3 plants) and grasses (C_4 plants in the study area). The sum of the long-chain *n*-alkanes (C_{27}-C_{33}) varies between 45 μg/g TOC and 260 μg/g TOC, showing the highest fluctuations in the early Holocene after 5.2 ka BP (**Supplementary Table S1**). CPI values are generally high and range between 7.6 and 4.8 (**Supplementary Table S1**), indicating no major contribution from fossil sources that might bias compound-specific δD and $\delta^{13}C$ values.

3.2. *n*-Alkane δD Values

δD values of the most abundant *n*-C_{29} and *n*-C_{31} plant wax homologues vary between –130 and –179‰ and thus exhibit a wide range of almost 50‰ (**Figure 3B**, **Supplementary Table S1**), which is comparable to the record of Lake Tana (~60‰; Costa et al., 2014). The similar δD evolution of the two homologues (r^2 = 0.95) suggests only a minor effect of vegetation changes (C_3 vs. C_4) on the climatic signal. We thus calculated δD_{wax} as the weighted average of both signals (**Supplementary Table S1**). The Younger Dryas (YD) is characterized by relatively positive δD_{wax} values (between –131 and –142‰). A rapid decrease of about 30‰ at 11.7 ka BP marks the abrupt termination of the YD. A second decrease of about 20‰ at 10 ka BP is followed by a ca. 2 kyr period with relatively stable δD values around –175‰. From ~8 ka BP, δD_{wax} values exhibit a long-term gradual increase to ca. 130‰ at about 2 ka BP. δD_{wax} values then decrease about 10‰ to the present, with some distinct fluctuations (**Figure 3B**). Late Holocene δD_{wax} values of Lake Dendi are comparable with modern δD_{wax} values reported for the Ethiopian highlands at a similar elevation (Jaeschke et al., 2018). In monsoon regions, variations in rainfall δD values are mainly controlled by the amount effect, with more negative δD values indicating more humid conditions. Different moisture sources potentially also influence precipitation δD values in the Ethiopian highlands (Rozanski et al., 1993; Levin et al., 2009). According to Costa et al. (2014), a contribution of 30% (modern) Congo-sourced moisture corresponds to a –4‰ change in δD, while in the most extreme case of 100% moisture derived from the Congo Basin could result in a δD change of –14‰. However, changes in the relative contribution of the different sources were proposed to be unrelated to the net annual precipitation amount (Costa et al., 2014). Here, we assume that δD_{wax} values primarily reflect the isotopic composition of local rainfall during the growing season (e.g., Schefuß et al., 2005) but also integrate the history of moisture transported to the Lake Dendi area, i.e., continental and Indian Ocean moisture.

3.3. $\delta^{13}C$ Values and Vegetation Types

n-Alkane $\delta^{13}C$ values range between –26.8 and –21.6‰ (*n*-C_{31}) and between –28.5 and 25.6‰ (*n*-C_{29}) (**Figure 3C**, **Supplementary Table S1**). The more ^{13}C-enriched values of the C_{31} *n*-alkane may be explained by the higher relative contribution of this homologue from C_4 grasses. $\delta^{13}C$ values of *n*-C_{29} generally show little variation but slightly ^{13}C-enriched values are observed during the early Holocene until about 8 ka BP and during the late Holocene starting at about 2 ka BP. $\delta^{13}C$ values of *n*-C_{31} are generally more ^{13}C enriched, especially from 9 to 8 ka BP and from 6.5 to 5 ka BP, resulting in a maximum isotopic spread of about 4‰ between *n*-C_{29} and *n*-C_{31} (**Figure 3C**). To estimate the relative contributions of C_4 and C_3 plants, which are dominantly controlled by aridity (Schefuß et al., 2003; Castañeda et al., 2009), a simplified two end-member mixing model is applied assuming end-member values for C_3 and C_4 vegetation of -34.7 and –21.4‰ for *n*-C_{29} and –35.2 and –21.7‰ for *n*-C_{31}, respectively (Castañeda et al., 2009; Berke et al., 2012b). Based on this assumption, the Lake Dendi region has a C_4-dominated (ca. 60–80%) vegetation (**Supplementary Table S1**). Uncertainties in the C_3/C_4 estimates of about 20%, however, have to be considered (Castañeda et al., 2009).

3.4. Pollen Stratigraphy

A total of 56 pollen and spore types was distinguished and percentages for the most abundant pollen taxa are summarized in **Figure 4**. Most important pollen groups indicating a C_4 plant origin are those of the grass (Poaceae) and sedge (Cyperaceae) families, while those from woody plants (*Podocarpus*, *Juniperus*) indicate a C_3 metabolism.

Poaceae pollen percentages are high throughout the record accounting for on average 62% during the YD, 53% throughout the AHP, and 32% during the late Holocene, (**Figure 4**). Cyperaceae pollen percentages range between 4 and 34%. Other herbaceous taxa include Asteraceae (av. 0.8–13.6%) and Amaranthaceae/Chenopodiaceae (av. 0.4–21.4%), Rosaceae (0.2–4.3%), Caryophyllaceae (0.2–5.3%), Solanaceae (0.2–2.5%), Apiaceae (0.2–2.6%), Fabaceae (0.2–2.5%) (**Figure 4**). High pollen percentages of Plantaginaceae (15–19%) are recorded only during the last 1,000 years (**Figure 4**) and may reflect the increasing anthropogenic influence in the Ethiopian highlands (Hamilton, 1982; Darbyshire et al., 2003; Umer et al., 2007; Hailu et al., 2015). Low pollen percentages of the dry Afromontane forest taxa *Podocarpus* are observed during both the YD and peak AHP (3–7%), while constantly increasing from ca. 7 ka BP to maximum values of 29% at 2.4 ka BP (**Figure 4**). Likewise, *Juniperus* pollen percentages increase over the course of the mid Holocene and reach a maximum of 19% at ca 3 ka BP, slightly leading those of *Podocarpus*. Other woody plant taxa are minor, i.e., Oleaceae (0.2–7%), Myricaceae (0.1–4%), Capparaceae (0.3–3%) (**Figure 4**).

The most distinct change in pollen distribution is observed above a ca. 2 m thick tephra layer, deposited at approximately 10.2 ka BP (**Figure 2**), and points to an extreme shift in plant community (**Figure 4**). This can be interpreted as the pioneer stage established after the volcanic eruption of Mount Wenchi located in close vicinity to Mount Dendi (**Figure 1B**) (Brown and Fuller, 2008; Wagner et al., 2018). Moreover, low pollen counts indicate sparse vegetation cover dominated by herbaceous plants. This extreme event may also have impacted the $\delta^{13}C$ and δD composition of the specific pioneer vegetation. Different photosynthetic pathways (C_3 vs. C_4 type) and diverse growth forms (e.g., trees, shrubs vs. herbaceous plants) vary in terms of stable carbon isotopic composition (Vogts et al., 2009; Jaeschke et al., 2018) and discriminate differently against deuterium during

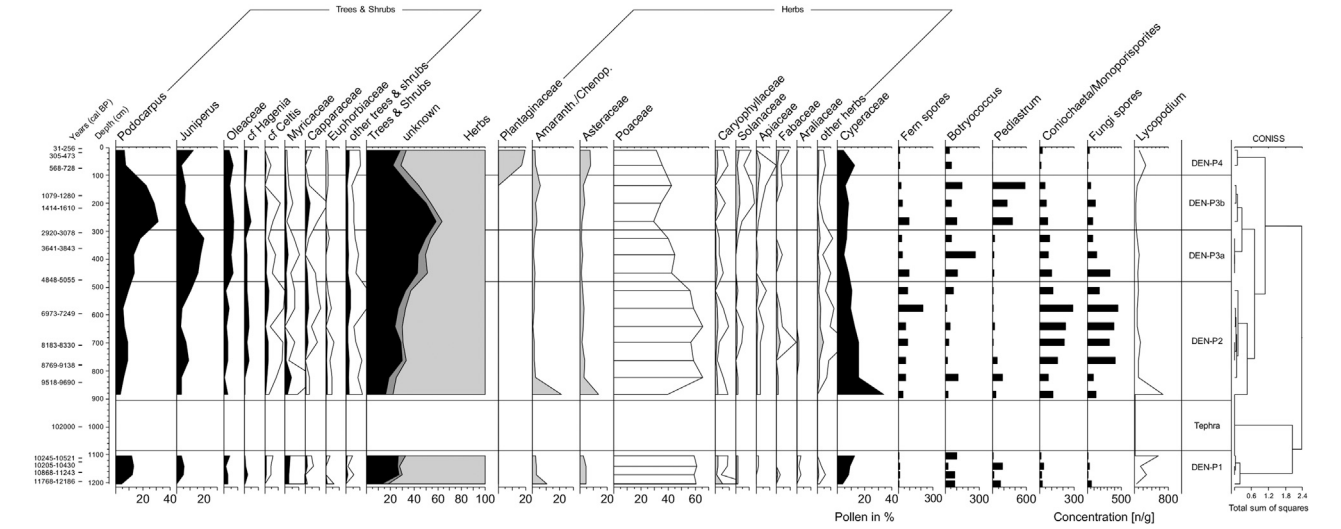

FIGURE 4 | Pollen diagram from Lake Dendi, showing percentage abundances of the principal taxa on a calibrated radiocarbon timescale. Percentages are calculated from the sum of all pollen grains (Cyperaceae excluded). The concentration of the palynomorphes was calculated based on the sediment dry weight.

lipid synthesis (Sachse et al., 2012). This may either amplify or reduce the signal. Both, $\delta^{13}C$ and δD values show abrupt shifts (**Figures 3B,C**) that coincide with the deposition of tephra at 10.2 ka BP and may thus not necessarily reflect a climatic signal.

4. DISCUSSION

4.1. Hydroclimate Changes at Lake Dendi and East Africa

The δD_{wax} record from Lake Dendi indicates that the Ethiopian highlands experienced major changes in hydroclimate during the past 12,500 years (**Figures 3B**, **5D**). Arid conditions during the YD documented at many Northeast and East African sites (Tierney et al., 2011; Foerster et al., 2012; Junginger et al., 2014; Castañeda et al., 2016) are confirmed at Lake Dendi by our δD_{wax} record (**Figure 5D**) and other sedimentological data (Wagner et al., 2018). Across tropical Africa, the termination of the YD was marked by an abrupt change in hydroclimate which involved major reorganization of monsoonal circulation across the continent and adjacent oceans (Talbot et al., 2007). Intense NH heating and an associated increase in thermal contrast between land and ocean resulted in a strengthening of the West African Monsoon (WAM) and the Indian Summer Monsoon (ISM) allowing the northward expansion of the tropical rainbelt (Nicholson, 2017; Pausata et al., 2020). The abruptness of change is thought to be related to the rapid resumption of the Atlantic Meridional Overturning Circulation (AMOC) (McManus et al., 2004; Weldeab et al., 2014). At Lake Dendi, the onset of the AHP and increasing rainfall at 11.7 ka BP are characterized by a large and abrupt shift in δD_{wax} of ~30‰ (**Figure 5D**). This abrupt decrease in δD_{wax} that points to increasing rainfall is in line with the abrupt strengthening of the WAM as indicated by the Ba/Ca time series from a marine sediment core of the Gulf of Guinea (Weldeab et al., 2007) (**Figure 5E**). A more gradual intensification of the monsoon circulation was indicated by Ba/Ca from a sediment core of the Levantine Sea and was proposed to reflect the influence of moisture from the Western Indian Ocean (Weldeab et al., 2014). Maximum monsoon rainfall at 9.9 ka BP and thus highest Nile river runoff based on Ba/Ca (**Figure 5C**) is in line with highest precipitation over the Blue Nile river basin as recorded in Lake Dendi δD_{wax} (**Figure 5D**). The timing of maximum rainfall at Lake Dendi is also in line with the abrupt intensification of the ISM based on the Qunf Cave $\delta^{18}O$ record from Oman (Fleitmann et al., 2003) (**Figure 5B**). The increased precipitation in the ISM domain corresponds to an enhanced atmospheric pressure gradient between East Africa and India (Camberlin, 1997; Junginger et al., 2014) that also leads to advection of D-depleted moisture from westerly sources, i.e. by an eastward shift of the CAB (Levin et al., 2009; Kebede and Travi, 2012; Costa et al., 2014). The incursion of humid air masses from the Congo Basin thus likely increased precipitation amount and decreased precipitation δD values in the Dendi area. Peak AHP conditions at Lake Dendi documented by strongly depleted δD_{wax} values of around −175‰ between 10 and 8 ka BP align with maximum NH insolation (Berger and Loutre, 1991) (**Figure 5A**) and highest monsoon intensity based on different archives (Fleitmann et al., 2003; Weldeab et al., 2007; Weldeab et al., 2014). This humid interval at the end of the early Holocene is also well-documented in other Northeast and East African hydroclimate records (Gasse, 2000; Tierney et al., 2011; Berke et al., 2012b; Foerster et al., 2012; Tierney and deMenocal, 2013; Costa et al., 2014; Castañeda et al., 2016), however, with locally different timing of onset and termination of the AHP (**Figure 6**). Intensified precipitation over the Blue Nile catchment area (**Figures 6D,E**) is also indicated by enhanced river discharge

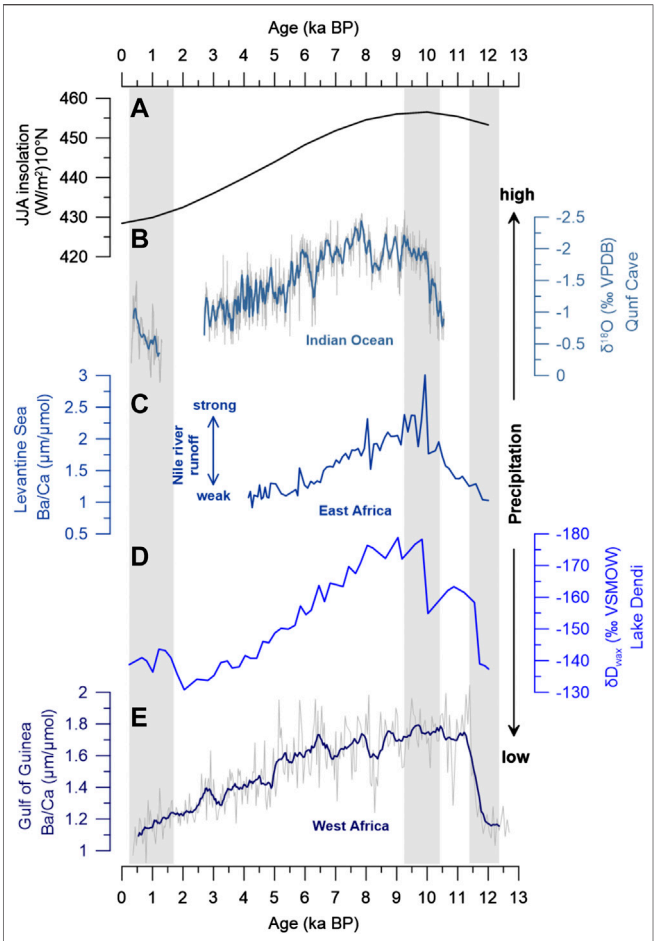

FIGURE 5 | Comparison with monsoon precipitation records. **(A)** Mean JJA insolation at 10°N (Berger and Loutre, 1991). **(B)** Stalagmite $\delta^{18}O$ record from Oman indicating changes in Indian Summer Monsoon (Fleitmann et al., 2003). **(C)** Ba/Ca record from the Levantine Basin indicating changes in Nile River discharge related to East African Monsoon rainfall (Weldeab et al., 2014). **(D)** Lake Dendi δD_{wax} record indicating changes in rainfall in the Ethiopian highlands (this study). **(E)** Ba/Ca record from the Gulf of Guinea indicating changes in river runoff draining the West African Monsoon area (Weldeab et al., 2007). Vertical gray bars mark abrupt changes in the monsoon systems based on the different proxies.

based on sedimentary records from the Nile deep-sea fan and eastern Mediterranean Sea (Blanchet et al., 2014; Castañeda et al., 2016). At the height of Nile River runoff, archaeological records indicate the abandonment of prehistoric human settlements in the Nile valley (Kuper and Kröpelin, 2006) while hydroclimate conditions were favourable for human occupation in the southern Sahara (Sereno et al., 2008) (**Figure 3A**).

After approximately 8 ka BP, the Lake Dendi δD_{wax} record shows a gradual aridification until ~2 ka BP, which is expressed in a progressive D-enrichment of ca. 45‰ (**Figure 5D**). The gradual decline in precipitation is in accordance with the long-term weakening of the African and Indian monsoon systems in response to decreasing NH summer insolation (Fleitmann et al., 2003; Weldeab et al., 2007; Weldeab et al., 2014) (**Figure 5**). This is supported by a general reduction in rainfall runoff based on sedimentological data at Lake Dendi (Wagner et al., 2018) and Lake Chew Bahir in southern Ethiopia (Foerster et al., 2012). A similar gradual trend in δD_{wax} is also observed in Lake Victoria, Kenya (Berke et al., 2012b) (**Figure 6F**) and in a sediment core from the eastern Mediterranean Sea (Castañeda et al., 2016) (**Figure 6B**), which received material from both, Blue and White Nile. Other δD_{wax} records from East Africa indicate continuous wet conditions during the AHP which ended abruptly at ~5 ka (Tierney et al., 2010; Tierney et al., 2011) (**Figures 6G,H**). Lakes Challa and Tanganyika located south of the equator experience a bimodal rainfall regime and may have benefited from enhanced short rains during autumn (Oct-Nov) related to SST anomalies in the Western Indian Ocean (Ummenhofer et al., 2009; Kuhnert et al., 2014). In contrast, the δD_{wax} record from Lake Tana, Ethiopia's largest lake, suggests an abrupt and early termination of the AHP at ~8.5 ka (Costa et al., 2014) (**Figure 6D**). The authors attributed this abrupt shift in δD_{wax} of about 60‰ to the westward retreat of the CAB and thus reduced moisture with a D-depleted signature derived from westerly sources (Congo Basin). Lake Dendi is located ~300 km to the south of Lake Tana, therefore, an abrupt shift of the CAB should have influenced δD_{wax} in a similar manner. We suspect locally different responses to changing hydroclimate associated with the 8.2 ka cold event in the North Atlantic (Alley and Ágústsdóttir, 2005). A distinct dry period between 8.5 and 7.8 ka has been documented by various archives throughout East Africa. Low lake levels were indicated in Lakes Ziway-Shala and Abhé (Gasse, 2000), Lakes Turkana and Suguta (Garcin et al., 2012; Junginger et al., 2014), Lake Tana (Marshall et al., 2011) and Chew Bahir (Foerster et al., 2012). Blanchet et al. (2014) suggested that this dry event marked a permanent modification of erosion dynamics and vegetation cover. Likewise, a decrease in Nile River runoff at 8.6–8.2 ka was reported based on Ba/Ca and Fe/Ca (Weldeab et al., 2014; Revel et al., 2010) and Sr isotopes (Blanchet et al., 2014) (**Figure 7A**). During this period, the southward migration of the rainbelt together with weakened monsoon precipitation in response to the 8.2 ka cold event may still have reached Lake Dendi, while Lake Tana dried out. In addition, a generally lower lake level of Lake Tana and lower elevation (i.e., implementing higher air temperature) would favor desiccation (drought stress) compared to Lake Dendi. Although not clearly visible from δD_{wax}, ^{13}C-enriched values of the *n*-alkanes may indicate the sensitive plant response to small changes in the local moisture balance at Lake Dendi during this interval (**Figure 3C**).

Late Holocene climate in East Africa is characterized by arid conditions in response to minimum NH summer insolation and a decrease in monsoon rainfall (**Figure 5**). According to the Lake Dendi δD_{wax} record, maximum aridity in the Ethiopian highlands is reached at ~2 ka BP (**Figures 3**, **6E**). This is in good agreement with the δD_{wax} record of Lake Tana (**Figure 6D**), the source of the Blue Nile (Costa et al., 2014). During the last 1,500 years, a trend toward slightly increasing humidity is indicated by a –15‰ shift in δD_{wax} (**Figure 5D**). This overall climatic rebound might be connected to a higher influence of precipitation from the Atlantic/Congo Basin as followed by a re-strengthening of the ISM (Fleitmann et al., 2003) (**Figure 5B**). The re-establishment of

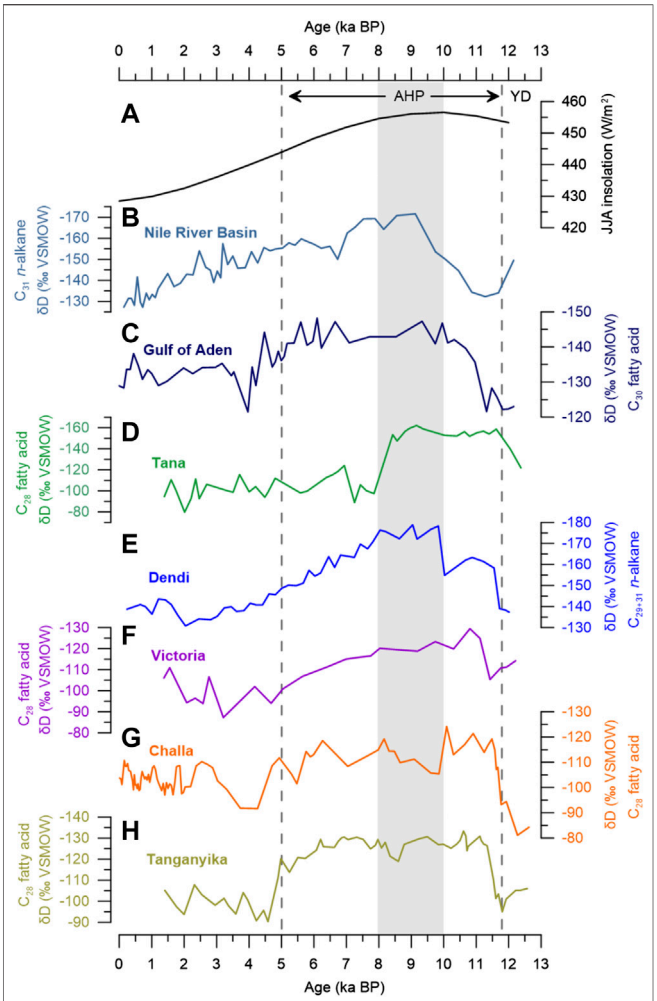

FIGURE 6 | Comparison with other East African δD_{wax} records. **(A)** Mean JJA insolation at 10°N (Berger and Loutre, 1991). **(B)** Nile River Basin (Castañeda et al., 2016). **(C)** Gulf of Aden (Tierney and deMenocal, 2013). **(D)** Lake Tana (Costa et al., 2014). **(E)** Lake Dendi (this study). **(F)** Lake Victoria (Berke et al., 2012b). **(G)** Lake Challa (Tierney et al., 2011). **(H)** Lake Tanganyika (Tierney et al., 2010). Vertical gray bar marks the optimum of the African Humid Period (AHP) at Lake Dendi. Black arrows indicate extent of the AHP in Africa.

seasonal rainfall in the Blue Nile source region is also indicated by enhanced Nile river discharge based on radiogenic Sr isotopes (**Figure 7A**), however with less vigorous floods compared to the early Holocene (Blanchet et al., 2014). The high fluctuations in rainfall runoff reported for Lake Dendi (**Figure 7B**) (Wagner et al., 2018) are also visible in the plant wax records (**Figure 3B**). These might be related to natural short-term environmental changes during the last millennium including the Medieval Warm Period (MWP) and the Little Ice Age. Thus, slightly enriched δD_{wax} values indicating a decrease in rainfall coincides with the MWP, which is frequently associated with a more arid climate in East Africa (Bonnefille and Mohammed, 1994; Verschuren et al., 2000; De Cort et al., 2013).

In conclusion, the timing and pace of hydroclimate evolution at Lake Dendi during the Holocene occurred in synchrony with the strength of the African and Indian monsoon systems and thus precipitation amount, pointing to orbitally induced gradual changes in NH summer insolation as the dominant forcing (Fleitmann et al., 2003; Renssen et al., 2006; Liu et al., 2007; Weldeab et al., 2007; Weldeab et al., 2014; Claussen et al., 2013). In East Africa, the variability in the amplitude of changes in δD_{wax} during the AHP compared to the late Holocene may be linked to a zonal gradient of hydroclimate anomaly patterns associated with the migration of the CAB (Tierney et al., 2011; Costa et al., 2014; Junginger et al., 2014). At Lake Dendi, this change of about 40‰ likely integrates the effects of both precipitation amount and water vapor transport, which is also seen in other East African δD_{wax} records (Tierney et al., 2010; Berke et al., 2012b; Castañeda et al., 2016).

4.2. Vegetation Response to Hydroclimate Changes at Lake Dendi

The pollen records of Lake Dendi provide evidence of distinct vegetation changes that accompanied the climate history in the region (**Figures 4**, **7E,F**). A sparse vegetation cover dominated by drought-tolerant C_4 grasses in combination with low total pollen counts suggests dry conditions at the end of the YD associated with low temperatures in the highlands and low CO_2 levels (Ehleringer et al., 1997). This is in line with other East African pollen records (Barker and Gasse, 2003), including Lake Tana (Lamb et al., 2007), Lake Victoria (Johnson et al., 1996), and Lake Garba Guracha in the Bale Mountains (Umer et al., 2007). The onset of more humid conditions during the AHP, as indicated by our δD_{wax} record, is accompanied by an increase in pollen counts but generally minor changes in vegetation composition, suggested by the predominance of Poaceae pollen between ca. 11.5 and 6 ka BP (**Figures 4**, **7F**). This is also reflected in ^{13}C-enriched values indicative of C_4 plants (**Figure 3C**) and in line with our $\delta^{13}C$-based estimation of vegetation types in the Dendi catchment (**Supplementary Table S1**). At ~10 ka BP, however, ca. 200 years after the volcanic eruption of Mount Wenchi (Brown and Fuller, 2008; Wagner et al., 2018), a distinct change in vegetation composition in combination with generally low pollen counts points to a pioneer stage developed after deposition of tephra in the catchment (**Figure 4**).

While the δD_{wax} record indicates gradual aridification between ca. 8 and 2 ka BP in response to weakening insolation forcing of the monsoon strength and thus precipitation amount (**Figures 5**, **7C**), increasing tree pollen percentages until ca. 2.4 ka BP indicate the expansion of a dry montane forest in the Dendi catchment (**Figures 4**, **7E**). A similar trend is also reported for the Bale Mountains, but culminates as early as about 4.5 ka BP (Umer et al., 2007). The climatic change to late Holocene aridity is well known throughout northern and eastern Africa (Kuper and Kröpelin, 2006; Lézine et al., 2011a). The resulting increase in the dry montane forest taxa (i.e., *Podocarpus*, *Juniperus*, Oleaceae; **Figure 4**) is also widely expressed in the central East African highlands, where a distinct dry season exists at present (Hamilton, 1982; Umer et al., 2007). Specifically, *Juniperus* is known to be more drought-resilient compared to *Podocarpus* and can tolerate extremely low precipitation amounts of ~200 mm/

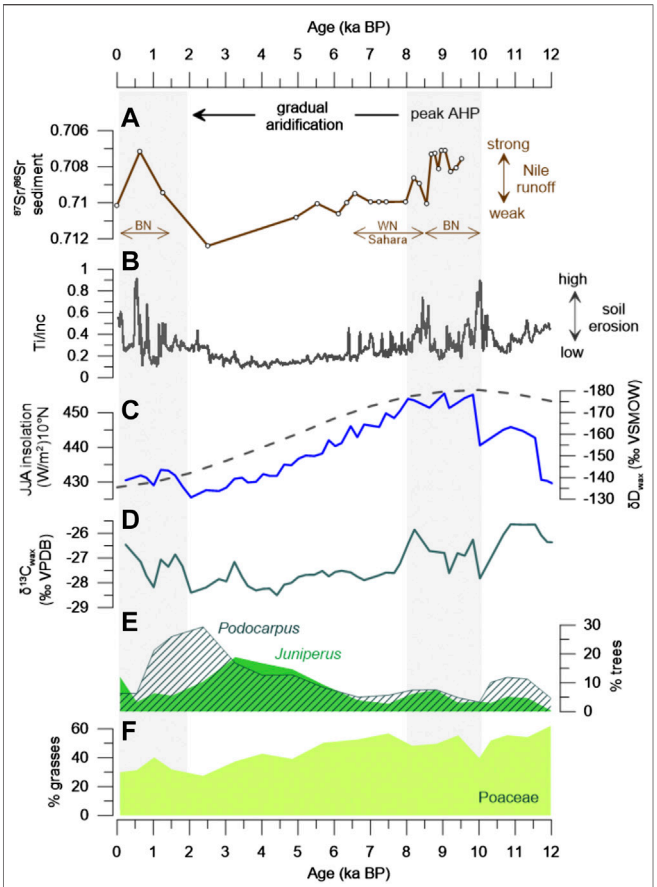

FIGURE 7 | Changes in precipitation and vegetation at Lake Dendi and river runoff in the Nile watershed during the Holocene. **(A)** Sediment sources from the Blue Nile (BN), White Nile (WN) and Sahara as estimated from the radiogenic Sr isotope signature in a marine sediment core from the Nile deep-sea fan (Blanchet et al., 2014). **(B)** Changes in catchment erosion at Lake Dendi based on Ti XRF-counts (Wagner et al., 2018). **(C)** Lake Dendi δD_{wax} record indicating changes in rainfall in the Ethiopian highlands (this study). Mean JJA insolation at 10°N (Berger and Loutre, 1991) is indicated as gray dashed line. **(D)** Lake Dendi $\delta^{13}C$ values of *n*-C_{29} indicate increasing contribution of C_3 vegetation (trees) from the late to the mid Holocene (this study). **(E)**, **(F)** Lake Dendi pollen percentages of predominant trees and grasses, respectively (this study). Vertical gray bars mark periods of enhanced Nile river runoff during high rainfall in the BN catchment.

year (Hall, 1984; Friis, 1992). Their increase, therefore, is believed to mark the establishment of the modern pattern of monsoonal rainfall seasonality (Umer et al., 2007).

Although the decline in insolation from its maximum during the early Holocene was gradual, many paleoclimatic records indicate an abrupt change to late Holocene aridity, explained as a triggering of vegetation albedo feedback mechanisms that provoke a nonlinear response to orbital forcing (DeMenocal et al., 2000; Renssen et al., 2006; Claussen et al., 2013). Vegetation is highly sensitive to the length of the dry season as well as the persistence of dry events (Lézine et al., 2011b). Specifically, length and intensity of the rainy season, dry spell occurrence and wind strength are of primary importance for plant distribution and pollen transport. However, the Lake Dendi pollen records show a gradual increase in both *Podocarpus* and *Juniperus* from ~6.5 ka BP onward (**Figures 4**, **7E**), which is in line with findings from the Bale Mountains (Umer et al., 2007). The gradual response may thus reflect the natural development of a dry Afromontane forest during the mid to late Holocene (Bonnefille and Hamilton, 1986; Darbyshire et al., 2003), related to the reduced precipitation in the region (**Figures 5**, **7C**). In combination with the pollen data we suggest that constantly decreasing $\delta^{13}C$ values of the *n*-C_{29} alkane (**Figure 7D**) may reflect the increasing contribution of C_3 woody plants. At the same time, the abundance of Poaceae pollen gradually decreased from 54% during the early to mid Holocene to 35% during the late Holocene (**Figure 7F**), pointing to a general reduction in understory grasses.

The maximum extent of trees and shrubs at Lake Dendi aligns with a minimum in precipitation amount in the source regions of the Blue Nile based on our δD_{wax} record (**Figures 6E**, **7C**) and that of Lake Tana (Costa et al., 2014) (**Figure 6D**). Most arid climate conditions in the Ethiopian highlands are corroborated by reduced catchment erosion at Lake Dendi (Wagner et al., 2018) (**Figure 7B**) and a strong reduction in Nile River discharge (Blanchet et al., 2014) (**Figure 7A**) as well as highest amounts of eolian dust detected in sediments of the Nile deep-sea fan (Blanchet et al., 2013). Increased dust transport during peak aridity may have facilitated eolian transport of *Podocarpus* pollen from additional extralocal sources (Hamilton, 1982) to the Dendi region (**Figure 7E**). On the other hand, highest pollen abundance of the more drought-tolerant *Juniperus* (**Figure 7E**), which are less susceptible to eolian transport, occurs earlier and aligns with the onset of full desert conditions at Lake Yoa at ~2.7 ka BP (Kröpelin et al., 2008). In East Africa, the late Holocene is characterized by increasing influence of human activity and a substantial land-cover change, which is also visible in the Ethiopian highlands (Hamilton, 1982; Friis, 1992; Darbyshire et al., 2003; Umer et al., 2007). At Lake Dendi, decreasing *Podocarpus* pollen percentages from about 1 ka BP point to tree clearance in favor of intensified agricultural use, which is indicated by high abundances of Plantaginaceae and Solanaceae pollen (**Figure 4**).

At high elevations, temperature is the main controlling factor allowing the growth of woody plants and for the establishment of open forest vegetation. Therefore, tropical warming during the Holocene may have extended the upper limit of trees toward higher altitudes in the Ethiopian highlands (Bonnefille and Mohammed, 1994; Wu et al., 2007). At Lake Dendi, the increase in pollen from drought-resilient taxa such as *Juniperus* and *Podocarpus* (**Figure 7E**) indicate the onset of forest development during the warm "Holocene Climate Optimum" (Wanner et al., 2011 and references therein). This pervasive mid Holocene warming is documented in lake sediment records from lower elevations in tropical East Africa (Powers et al., 2005; Tierney et al., 2010; Berke et al., 2012a). Distinct from most lowland savanna type vegetation that suffered degradation during the mid to late Holocene, the highlands received still sufficient moisture to support tree growth. A dense vegetation cover with more leaf litter and higher soil humus content may have restricted erosion of clastic minerals in the Dendi catchment (**Figure 7B**) (Wagner et al., 2018). In addition, high atmospheric CO_2

levels may have stabilized tropical forests by promoting tree growth, despite increased aridity (Shanahan et al., 2016). Our observations thus confirm model simulations by Claussen et al. (2013), that point to a substantial impact of plant diversity on the stability of the climate–vegetation system during the AHP transition. Our combined molecular and pollen records also indicate that vegetation evolution at Lake Dendi toward a dry montane forest is in line with the general trend in African hydroclimate evolution during the Holocene.

5. CONCLUSIONS

The Lake Dendi molecular and pollen records showed that Ethiopian highland vegetation was sensitive to moderate changes in moisture availability during the past 12,500 years. The gradual nature of hydroclimate change was related to weakening insolation forcing of the African and Indian Ocean monsoon intensities and thus precipitation amount. Based on our sedimentary δD_{wax} record, the onset of the AHP that followed YD aridity at Lake Dendi occurred in concert with the strengthening of the WAM at 11.7 ka BP. Peak AHP conditions were established at 10 ka BP, caused by the eastward shift of the CAB onto the central Ethiopian Plateau most likely due to an increase in ISM strength. After ca. 8 ka BP, the westward migration of the CAB resulted in a moderate decrease in precipitation amount, leading to a gradual transition out of the AHP. Peak aridity occurred around 2 ka BP, followed by a return to a generally wetter climate possibly linked to a re-strengthening of the ISM. The amplitude of change in δD_{wax} during the AHP compared to the late Holocene of about 40‰ is comparable to those of other East African δD_{wax} records influenced by the CAB. Parallel to the hydroclimate evolution, the vegetation structure at Lake Dendi changed gradually from a C_4-grass dominated vegetation toward the establishment of a dry montane forest characterized by *Juniperus*, *Podocarpus* and Oleaceae, which implies that moisture availability was not a limiting factor. At high elevations, rising temperatures and increasing atmospheric CO_2 levels during the Holocene may have initiated the growth of woody plants that once established, stabilized the vegetation cover, reduced soil erosion and sustained microclimate at Lake Dendi. During the last millennium, increasing anthropogenic activity is indicated by the pollen record pointing to deforestation and agriculture. Our results highlight that the nature of the transition out of the AHP seems to be controlled by complex interactions and shifts of wind regimes together with local insolation changes at different geographical positions. Finally, our multi-proxy approach showed that information on vegetation structure is important when interpreting plant wax-derived δD and $\delta^{13}C$ signatures.

DATA AVAILABILITY STATEMENT

All datasets generated in this study are included in the article and/or the Supplementary Files. Raw data are available in the PANGAEA repository (https://doi.pangaea.de/10.1594/PANGAEA.923143, https://doi.pangaea.de/10.1594/PANGAEA.923144).

AUTHOR CONTRIBUTIONS

FS and JR designed the research. FS and JU completed the sampling in Ethiopia. MT and ES carried out the lipid workup and compound-specific isotope analysis. JU carried out the pollen analysis. BW provided the age model. AJ completed data interpretation and served as primary author. All authors discussed the results and wrote the manuscript.

FUNDING

Funding for this study was provided by the German Research Foundation (DFG) within the scope of the CRC 806 ("Our way to Europe") - Project Number 57444011.

ACKNOWLEDGMENTS

We thank the editor and two reviewers for their helpful comments, which improved the quality of this manuscript. We would like to thank the whole coring team, Henry Lamb, Tamrat Endale, and Christian Tourney. Tamrat Endale and Asfawossen Asrat are thanked for logistic support during the field activities. We thank Ilona Steffen and Ralph Kreutz for help with sample preparation and isotope analysis.

SUPPLEMENTARY MATERIAL

The Supplementary Material for this article can be found online at: https://www.frontiersin.org/articles/10.3389/feart.2020.585770/full#supplementary-material.

REFERENCES

Alley, R. B. and Ágústsdóttir, A. M. (2005). The 8k event: cause and consequences of a major Holocene abrupt climate change. *Quat. Sci. Rev.* 24, 1123–1149. doi:10.1016/j.quascirev.2004.12.004

Barker, P. and Gasse, F. (2003). New evidence for a reduced water balance in East Africa during the Last Glacial Maximum: implication for model-data comparison. *Quat. Sci. Rev.* 22, 823–837. doi:10.1016/s0277-3791(03)00010-6

Bekele, T. (1993). "Vegetation ecology of remnant Afromontane forests on the central plateau of Shewa, Ethiopia," in *Acta phytogeographica Suecica*. Editor E. Sjörgen (Uppsala: Opulus Press AB), 3–64.

Berger, A. and Loutre, M. F. (1991). Insolation values for the climate of the last 10 million years. *Quat. Sci. Rev.* 10, 297–317. doi:10.1016/0277-3791(91)90033-q

Berke, M. A., Johnson, T. C., Werne, J. P., Schouten, S., and Sinninghe Damsté, J. S. (2012a). A mid-Holocene thermal maximum at the end of the African Humid Period. *Earth Planet Sci. Lett.* 351-352, 95–104. doi:10.1016/j.epsl.2012.07.008

Berke, M. A., Johnson, T. C., Werne, J. P., Grice, K., Schouten, S., and Sinninghe Damsté, J. S. (2012b). Molecular records of climate variability and vegetation response since the late pleistocene in the lake Victoria basin, east Africa. *Quat. Sci. Rev.* 55, 59–74. doi:10.1016/j.quascirev.2012.08.014

Blanchet, C. L., Frank, M., and Schouten, S. (2014). Asynchronous changes in vegetation, runoff and erosion in the Nile River watershed during the Holocene. *PloS One* 9 (12), e115958. doi:10.1371/journal.pone.0115958

Blanchet, C. L., Tjallingii, R., Frank, M., Lorenzen, J., Reitz, A., et al. (2013). High- and low-latitude forcing of the Nile River regime during the Holocene inferred from laminated sediments of the Nile deep-sea fan. *Earth Planet Sci. Lett.* 364, 98–110. doi:10.1016/j.epsl.2013.01.009

Bonnefille, R. (1971a). Atlas des pollens d'Ethiopie. Pollens actueles de la base vallée de l'Omo. *Adansonia* 2, 463–518.

Bonnefille, R. (1971b). Atlas des pollens d'Ethiopie. Principales espèces des forets de montagne. *Adansonia* 13, 15–72.

Bonnefille, R. and Hamilton, A. (1986). Quaternary and late tertiary history of Ethiopian vegetation. *Symb. Bot. Ups.* 26, 48–63.

Bonnefille, R. and Mohammed, U. (1994). Pollen-inferred climatic fluctuations in Ethiopia during the last 3000 years. *Palaeogeogr. Palaeoclimatol. Palaeoecol.* 109, 331–343. doi:10.1016/0031-0182(94)90183-x

Bonnefille, R. and Riollet, G. (1980). *Pollens des savanes d'Afrique orientale*. Paris, France:Editions du Centre National de la Recherche Scientifique, 140.

Bowen, G. J. (2008). Spatial analysis of the intra-annual variation of precipitation isotope ratios and its climatological corollaries. *J. Geophys. Res.* 113, D05113. doi:10.1029/2007JD009295

Bray, E. E. and Evans, D. E. (1961). Distribution of n-paraffins as a clue to recognition of source beds. *Geochem. Cosmochim. Acta* 22, 2–15. doi:10.1016/0016-7037(61)90069-2

Brown, F. H. and Fuller, C. R. (2008). Stratigraphy and tephra of the kibish formation, southwestern Ethiopia. *J. Hum. Evol.* 55, 366–403. doi:10.1016/j.jhevol.2008.05.009

Camberlin, P. (1997). Rainfall anomalies in the source region of the nile and their connection with the Indian summer monsoon. *J. Clim.* 10, 1380–1392. doi:10.1175/1520-0442(1997)010<1380:raitsr>2.0.co;2

Camberlin, P., Janicot, S., and Poccard, I. (2001). Seasonality and atmospheric dynamics of the teleconnection between African rainfall and tropical sea-surface temperature: Atlantic vs ENSO. *Int. J. Climatol.* 21, 973–1005.

Castañeda, I. S., Mulitza, S., Schefuß, E., Lopes Dos Santos, R., Sinninghe Damsté, J. S., and Schouten, S. (2009). Wet phases in the Sahara/Sahel region and human migration patterns in North Africa. *Proc. Natl. Acad. Sci. USA* 106, 20159–20163. doi:10.1002/joc.673

Castañeda, I. S. and Schouten, S. (2011). A review of molecular organic proxies for examining modern and ancient lacustrine environments. *Quat. Sci. Rev.* 30, 2851–2951. doi:10.1016/j.quascirev.2011.07.009

Castañeda, I. S., Schouten, S., Pätzold, J., Lucassen, F., Kasemann, S., Kuhlmann, H., et al. (2016). Hydroclimate variability in the Nile river basin during the past 28,000 years. *Earth Planet Sci. Lett.* 438, 47–56. doi:10.1016/j.epsl.2015.12.014

Claussen, M., Bathiany, S., Brovkin, V., and Kleinen, T. (2013). Simulated climate-vegetation interaction in semi-arid regions affected by plant diversity. *Nat. Geosci.* 6, 954–958. doi:10.1038/ngeo1962

Collins, J. A., Prange, M., Caley, T., Gimeno, L., Beckmann, B., Mulitza, S., et al. (2017). Rapid termination of the African Humid Period triggered by northern high-latitude cooling. *Nat. Commun.* 8, 1372. doi:10.1038/s41467-017-01454-y

Costa, K., Russell, J., Konecky, B., and Lamb, H. (2014). Isotopic reconstruction of the African humid period and Congo air boundary migration at Lake Tana, Ethiopia. *Quat. Sci. Rev.* 83, 58–67. doi:10.1016/j.quascirev.2013.10.031

Darbyshire, I., Lamb, H. F., and Umer, M. (2003). Forest clearance and regrowth in northern Ethiopia during the last 3000 years. *Holocene* 13, 537–546. doi:10.1191/0959683603hl644rp

De Cort, G., Bessems, I., and Keppens, E. (2013). Late-Holocene and recent hydroclimatic variability in the central Kenya Rift Valley: the sediment record of hypersaline lakes Bogoria, Nakuru and Elementeita. *Palaeogeogr. Palaeoclimatol. Palaeoecol.* 388, 69–80. doi:10.1016/j.palaeo.2013.07.029

Degefu, F., Herzig, A., Jirsa, F., and Schagerl, M. (2014). First limnological records of highly threatened tropical high-mountain crater lakes in Ethiopia. *Trop. Conserv. Sci.* 7 (3), 365–381. doi:10.1177/194008291400700302

DeMenocal, P., Ortiz, J., Guilderson, T., Adkins, J., Sarnthein, M., Baker, L., et al. (2000). Abrupt onset and termination of the African Humid Period: rapid climate responses to gradual insolation forcing. *Quat. Sci. Rev.* 19, 347–361. doi:10.1016/s0277-3791(99)00081-5

Dupont, L. M. and Schefuß, E. (2018). The roles of fire in Holocene ecosystem changes off West Africa. *Earth Planet Sci. Lett.* 481, 255–263. doi:10.1016/j.epsl.2017.10.049

Eglinton, T. I. and Eglinton, G. (2008). Molecular proxies for paleoclimatology. *Earth Planet Sci. Lett.* 275, 1–16. doi:10.1016/j.epsl.2008.07.012

Ehleringer, J. R., Cerling, T. E., and Helliker, B. R. (1997). C4 photosynthesis, atmospheric CO2, and climate. *Oecologia* 112, 285–299. doi:10.1007/s004420050311

Faegri, K., Kaland, P. E., and Krzywinski, K. (1989). *Textbook of pollen analysis*. 4th Edn. Chichester, United Kingdom: John Wiley & Sons, 328.

Fleitmann, D., Burns, S. J., Mudelsee, M., et al. (2003). Holocene forcing of the Indian monsoon recorded in a stalagmite from southern Oman. *Science* 300, 1737–1739. doi:10.1126/science.1083130

Foerster, V., Junginger, A., Langkamp, O., Gebru, T., Asrat, A., Umer, M., et al. (2012). Climatic change recorded in the sediments of the Chew Bahir basin, southern Ethiopia, during the last 45,000 years. *Quat. Int.* 274, 25–37. doi:10.1016/j.quaint.2012.06.028

Friis, I. (1992). *Forests & forest trees of Northeast tropical Africa – their natural habitats and distribution patterns in Ethiopia, Djibouti and Somalia*. (London, United Kingdom: Royal Botanic Gardens), 396.

Friis, I., Demissew, S., and van Breugel, P. (2011). *Atlas of the potential vegetation of Ethiopia*. Addis Ababa, Ethiopia: Addis Ababa University Press and Shama Books.

Garcin, Y., Melnick, D., Strecker, M. R., Olago, D., and Tiercelin, J. J. (2012). East African mid-Holocene wet–dry transition recorded in palaeo-shorelines of Lake Turkana, northern Kenya Rift. *Earth Planet Sci. Lett.* 331-332, 322–334. doi:10.1016/j.epsl.2012.03.016

Gasse, F. (2000). Hydrological changes in the African tropics since the last glacial maximum. *Quat. Sci. Rev.* 19, 189–211. doi:10.1016/s0277-3791(99)00061-x

Gelorini, V., Verbeken, A., van Geel, B., Cocquyt, C., and Verschuren, D. (2011). Modern non-pollen palynomorphs from East African lake sediments. *Rev. Palaeobot. Palynol.* 164, 143–173. doi:10.1016/j.revpalbo.2010.12.002

Grimm, M. (2015). Tilia 2.0.41. Available at: http://www.tiliait.com/.

Hailu, B. T., Maeda, E. E., Heiskanen, J., and Pellikka, P. (2015). Reconstructing pre-agricultural expansion vegetation cover of Ethiopia. *Appl. Geogr.* 62, 357–365. doi:10.1016/j.apgeog.2015.05.013

Hall, J. B. (1984). Juniperus excelsa in Africa: a biogeographical study of an Afromontane tree. *J. Biogeogr.* 11, 47–61. doi:10.2307/2844775

Hamilton, A. C. (1982). *Environmental history of East Africa*. London, United Kingdom: Academic Press.

Höpker, S. N., Wu, H. C., Müller, P., Barusseau, J.-P., Vernet, R., Lucassen, F., et al. (2019). Pronounced northwest African monsoon discharge during the mid- to late Holocene. *Front. Earth Sci.* 7, 314. doi:10.3389/feart.2019.00314

Jaeschke, A., Rethemeyer, J., Lappé, M., Schouten, S., Boeckx, P., and Schefuß, E. (2018). Influence of land use on the distribution of soil n-alkane D and brGDGTs along an altitudinal transect in Ethiopia: implications for (paleo) environmental studies. *Org. Geochem.* 124, 77–87.

Johnson, T. C., Scholz, C. A., Talbot, M. R., Kelts, K., Ricketts, R. D., Ngobi, G., et al. (1996). Late Pleistocene desiccation of Lake Victoria and rapid evolution of cichlid fishes. *Science* 273, 1091–1093.

Junginger, A., Roller, S., Olaka, L. A., and Trauth, M. H. (2014). The effects of solar irradiation changes on the migration of the Congo Air Boundary and water levels of paleo-Lake Suguta, Northern Kenya Rift, during the African Humid Period (15–5 ka BP). *Palaeogeogr. Palaeoclimatol. Palaeoecol.* 396, 1–16.

Kahmen, A., Schefuß, E., and Sachse, D. (2013). Leaf water deuterium enrichment shapes leaf wax n-alkane δD values of angiosperm plants I: experimental evidence and mechanistic insights. *Geochem. Cosmochim. Acta* 111, 39–49. doi:10.1016/j.gca.2012.09.003

Kebede, S. and Travi, Y. (2012). Origin of the δ18O and δ2H composition of meteoric waters in Ethiopia. *Quat. Bar Int.* 257, 4–12. doi:10.1016/j.quaint.2011.09.032

Kröpelin, S., Verschuren, D., Lézine, A. M., Eggermont, H., Cocquyt, C., Francus, P., et al. (2008). Climate-driven ecosystem succession in the Sahara: the past 6000 years. *Science* 320, 765–768. doi:10.1126/science.1154913

Kuechler, R. R., Schefuß, E., Beckmann, B., Dupont, L., and Wefer, G. (2013). NW African hydrology and vegetation during the Last Glacial cycle reflected in plant-wax- specific hydrogen and carbon isotopes. *Quat. Sci. Rev.* 82, 56–67. doi:10.1016/j.quascirev.2013.10.013

Kuhnert, H., Kuhlmann, H., Mohtadi, M., Meggers, H., Baumann, K. H., and Pätzold, J. (2014). Holocene tropical western Indian Ocean sea surface temperatures in covariation with climatic changes in the Indonesian region. *Paleoceanography* 29, 423–437. doi:10.1002/2013pa002555

Kuper, R. and Kröpelin, S. (2006). Climate-controlled Holocene occupation in the Sahara: motor of Africa's evolution. *Science* 313, 803–807. doi:10.1126/science.1130989

Lamb, H. F., Bates, C. R., Coombes, P. V., Marshall, M. H., Umer, M., Davies, S. J., et al. (2007). Late pleistocene desiccation of Lake Tana, source of the blue Nile. *Quat. Sci. Rev.* 26, 287–299. doi:10.1016/j.quascirev.2006.11.020

Levin, N. E., Zipser, E. J., and Cerling, T. E. (2009). Isotopic composition of waters from Ethiopia and Kenya: insights into moisture sources for eastern Africa. *J. Geophys. Res.* 114, D23306. doi:10.1029/2009JD012166

Lézine, A. M., Casanova, J., and Hillaire-Marcel, C. (1990). Across an early Holocene humid phase in Western Sahara: pollen and isotope stratigraphy. *Geology* 18, 264–267. doi:10.1130/0091-7613(1990)018<0264:aaehhp>2.3.co;2

Lézine, A.-M., Hély, C., Grenier, C., Braconnot, P., and Krinner, G. (2011a). Sahara and Sahel vulnerability to climate changes, lessons from Holocene hydrological data. *Quat. Sci. Rev.* 30, 3001–3012. doi:10.1016/j.quascirev.2011.07.006

Lézine, A. M., Zheng, W., Braconnot, P., and Krinner, G. (2011b). Late Holocene plant and climate evolution at Lake Yoa, northern Chad: pollen data and climate simulations. *Clim. Past* 7, 1351–1362.

Liu, Z., Wang, Y., Gallimore, R., Gasse, F., Johnson, T., de Menocal, P., et al. (2007). Simulating the transient evolution and abrupt change of Northern Africa atmosphere-ocean-terrestrial ecosystem in the Holocene. *Quat. Sci. Rev.* 26, 1818–1837. doi:10.1016/j.quascirev.2007.03.002

Marshall, M. H., Lamb, H. F., Huws, D., Davies, S. J., Bates, R., and Bloemendal, J. (2011). Late pleistocene and Holocene drought events at Lake Tana, the source of the blue Nile. *Global Planet. Change* 78, 147–161. doi:10.1016/j.gloplacha.2011.06.004

McManus, J. F., Francois, R., Gherardi, J. M., Keigwin, L. D., and Brown-Leger, S. (2004). Collapse and rapid resumption of Atlantic meridional circulation linked to deglacial climate changes. *Nature* 428, 834–837. doi:10.1038/nature02494

Mitchell, T. D. and Jones, P. D. (2005). An improved method of constructing a database of monthly climate observations and associated high-resolution grids. *Int. J. Climatol.* 25, 693–712. doi:10.1002/joc.1181

Nicholson, S. E. (2017). Climate and climatic variability of rainfall over eastern. *Africa. Rev. Geophys.* 55, 590–635. doi:10.1002/2016rg000544

Nicholson, S. E. (2000). The nature of rainfall variability over Africa on time scales of decades to millenia. *Global Planet. Change* 26, 137–158. doi:10.1016/s0921-8181(00)00040-0

Pausata, F. S. R., Gaetani, M., Messori, G., Berg, A., Maia de Souza, D., Sage, R. F., et al. (2020). The greening of the Sahara: past changes and future implications. *One Earth* 2, 235–250. doi:10.1016/j.oneear.2020.03.002

Powers, L. A., Johnson, T. C., Werne, J. P., Castañeda, I., Hopmans, E. C., Sinninghe Damsté, J. S., et al. (2005). Large temperature variability in the southern African tropics since the last glacial maximum. *Geophys. Res. Lett.* 32, L08706. doi:10.1029/2004GL022014

Renssen, H., Brovkin, V., Fichefet, T., and Goosse, H. (2006). Simulation of the Holocene climate evolution in northern Africa: the termination of the African humid period. *Quat. Int.* 15, 95–102. doi:10.1016/j.quaint.2005.01.001

Revel, M., Ducassou, E., Grousset, F. E., Bernasconi, S. M., Migeon, S., Revillon, S., et al. (2010). 100,000 Years of African monsoon variability recorded in sediments of the Nile margin. *Quat. Sci. Rev.* 29, 1342–1362. doi:10.1016/j.quascirev.2010.02.006

Rozanski, K., Araguás-Araguás, L., and Gonfiantini, R. (1993). "Isotopic patterns in modern global precipitation," in *Climate change in continental isotopic records*. Editors P. K. Swart, K. C. Lohmann, J. McKenzie, and S. Savin (Washington, Unites States: American Geophysics Union), 79–93.

Sachse, D., Billault, I., Bowen, G. J., Chikaraishi, Y., Dawson, T. E., Feakins, S. E., et al. (2012). Molecular paleohydrology: interpreting the hydrogen-isotopic composition of lipid biomarkers from photosynthesizing organisms. *Ann. Rev. Earth Planet. Sci.* 40, 221–249. doi:10.1146/annurev-earth-042711-105535

Schefuß, E., Schouten, S., Jansen, J. F., and Sinninghe Damsté, J. S. (2003). African vegetation controlled by tropical sea surface temperatures in the mid-Pleistocene period. *Nature* 422 (6930), 418–421. doi:10.1038/nature01500

Schefuß, E., Schouten, S., and Schneider, R. R. (2005). Climatic controls on central African hydrology during the past 20,000 years. *Nature* 437, 1003–1006. doi:10.1038/nature03945

Sereno, P. C., Garcea, E. A. A., Jousse, H., Stojanowski, C., Saliège, J. F., Maga, A., et al. (2008). Lakeside cemeteries in the Sahara: 5000 Years of Holocene population and environmental change. *PloS One* 3, e2995. doi:10.1371/journal.pone.0002995

Shanahan, T. M., Hughen, K. A., Mckay, N. P., Overpeck, J. T., Scholz, C. A., Gosling, W. D., et al. (2016). CO2 and fire influence tropical ecosystem stability in response to climate change. *Sci. Rep.* 6, 29587. doi:10.1038/srep29587

Shanahan, T. M., McKay, N. P., Hughen, K. A., Overpeck, J. T., Otto-Bliesner, B., Heil, C. W., et al. (2015). The time-transgressive termination of the African humid period. *Nat. Geosci.* 8, 140–144. doi:10.1038/ngeo2329

Smith, F. A. and Freeman, K. H. (2006). Influence of physiology and climate on δD of leaf wax n-alkanes from C3 and C4 grasses. *Geochem. Cosmochim. Acta* 70, 1172–1187. doi:10.1016/j.gca.2005.11.006

Stanley, J. D., Krom, M. D., Cliff, R. A., and Woodward, J. C. (2003). Short contribution: Nile flow failure at the end of the Old Kingdom, Egypt: strontium isotopic and petrologic evidence. *Geoarchaeology* 18 (3), 395–402. doi:10.1002/gea.10065

Talbot, M. R., Filippi, M. L., Jensen, N. B., and Tiercelin, J. J. (2007). An abrupt change in the African monsoon at the end of the younger Dryas. *G-cubed* 8, Q03005. doi:10.1029/2006GC001465

Tierney, J. E. and deMenocal, P. B. (2013). Abrupt shifts in horn of Africa hydroclimate since the last glacial maximum. *Science* 342, 843–846. doi:10.1126/science.1240411

Tierney, J. E., Pausata, F. S. R., and deMenocal, P. B. (2017). Rainfall regimes of the Green Sahara. *Sci. Adv.* 3, e1601503. doi:10.1126/sciadv.1601503

Tierney, J. E., Russell, J. M., and Huang, Y. (2010). A molecular perspective on Late Quaternary climate and vegetation change in the Lake Tanganyika basin, East Africa. *Quat. Sci. Rev.* 29, 787–800. doi:10.1016/j.quascirev.2009.11.030

Tierney, J. E., Russell, J. M., Sinninghe Damsté, J. S., Huang, Y., and Verschuren, D. (2011). Late quaternary behavior of the east African monsoon and the importance of the Congo air boundary. *Quat. Sci. Rev.* 30, 798–807. doi:10.1016/j.quascirev.2011.01.017

Trenberth, K. E., Stepaniak, D. P., and Caron, J. (2000). The global monsoon as seen through the divergent atmospheric circulation. *J. Clim.* 13, 3969–3993. doi:10.1175/1520-0442(2000)013<3969:tgmast>2.0.co;2

Umer, M., Lamb, H. F., Bonnefille, R., Tiercelin, J. J., Gibert, E., Cazet, J. P., et al. (2007). Late pleistocene and Holocene vegetation history of the Bale mountains, Ethiopia. *Quat. Sci. Rev.* 26, 2229–2246. doi:10.1016/j.quascirev.2007.05.004

Ummenhofer, C. C., Gupta, A. S., and England, M. H. (2009). Contributions of Indian Ocean sea surface temperatures to enhanced east Africa rainfall. *J. Clim.* 22, 993–1013. doi:10.1175/2008jcli2493.1

Van Geel, B., Gelorini, V., Lyaruu, A., Aptroot, A., Rucina, S., Marchant, R., et al. (2011). Diversity and ecology of tropical African fungal spores from a 25,000-year palaeoenvironmental record in southeastern Kenya. *Rev. Palaeobot. Palynol.* 164, 174–190. doi:10.1016/j.revpalbo.2011.01.002

Verschuren, D., Laird, K. R., and Cumming, B. F. (2000). Rainfall and drought in equatorial east Africa during the past 1,100 years. *Nature* 403, 410–414. doi:10.1038/35000179

Vogelsang, R., Bubenzer, O., Kehl, M., Meyer, S., Richter, J., and Zinaye, B. (2018). When hominins conquered highlands—an Acheulean site at 3000 m a.s.l. on Mount Dendi/Ethiopia. *J. Paleol. Archaeol* 1, 302–313. doi:10.1007/s41982-018-0015-9

Vogts, A., Moossen, H., Rommerskirchen, F., and Rullkötter, J. (2009). Distribution patterns and stable carbon isotopic composition of alkanes and alkan-1-ols from plant waxes of African rain forest and savanna C3 species. *Org. Geochem.* 40, 1037–1054. doi:10.1016/j.orggeochem.2009.07.011

Wagner, B., Wennrich, V., Viehberg, F., Junginger, A., Kolvenbach, A., Rethemeyer, J., et al. (2018). Holocene rainfall runoff in the central Ethiopian highlands and evolution of the River Nile drainage system as

revealed from a sediment record from Lake Dendi. *Global Planet. Change* 163, 29–43. doi:10.1016/j.gloplacha.2018.02.003

Wanner, H., Solomina, O., Grosjean, M., Ritz, S. P., and Jetel, M. (2011). Structure and origin of Holocene cold events. *Quat. Sci. Rev.* 30, 3109–3123. doi:10.1016/j.quascirev.2011.07.010

Weldeab, S., Lea, D. W., Schneider, R. R., and Anderson, N. (2007). 155,000 years of West African monsoon and ocean thermal evolution. *Science* 316, 1303–1307. doi:10.1126/science.1140461

Weldeab, S., Menke, V., and Schmiedl, G. (2014). The pace of East African monsoon evolution during the Holocene. *Geophys. Res. Lett.* 41, 2014GL059361. doi:10.1002/2014gl059361

Wu, H., Guiot, J., Brewer, S., Guo, Z., and Peng, C. (2007). Dominant factors controlling glacial and interglacial variations in the treeline elevation in tropical Africa. *Proc. Natl. Acad. Sci. USA* 104 (23), 9720–9724. doi:10.1073/pnas.0610109104

Conflict of Interest: The authors declare that the research was conducted in the absence of any commercial or financial relationships that could be construed as a potential conflict of interest.